Received 27 April 2023, accepted 22 May 2023, date of publication 26 May 2023, date of current version 7 June 2023.
Digital Object Identifier 10.1109/ACCESS.2023.3280423

RESEARCH ARTICLE

Metaheuristic-Based Optimization and Prototype Investigation of Low Frequency Metamaterial for Wireless Power Transfer Application

WEBSTER ADEPOJU[1], (Member, IEEE),
INDRANIL BHATTACHARYA[1], (Senior Member, IEEE), **MARY SANYAOLU**[2],
MUHAMMAD BIMA ENAGI[3], (Student Member, IEEE), **EBRAHIM NASR ESFAHANI**[1],
TRAPA BANIK[1], (Graduate Student Member, IEEE),
AND OLATUNJI ABIODUN[1], (Graduate Student Member, IEEE)
[1]Department of Electrical and Computer Engineering, Tennessee Technological University, Cookeville, TN 38505, USA
[2]GasFleet Engineering Ltd., Lagos 100267, Nigeria
[3]Nordstrom Inc., Atlanta, GA 30326, USA
Corresponding authors: Webster Adepoju (woadepoju42@tntech.edu) and Indranil Bhattacharya (ibhattacharya@tntech.edu)

ABSTRACT The adoption of wireless charging technologies for consumer and industrial applications is inhibited by concerns over reliability culminating from the fluctuating output power, low transmit power, and power transfer efficiency (PTE) of these systems. Besides, the inherently high radio and microwave resonant frequency of existing Metamaterial (MTM) designs imposes high switching stress on power switches and passive components, leading to significant power loss and enormously high degradation in system performance. This manuscript presents a compact, low-frequency MTM-based Wireless Power Transfer (WPT) structure coupled with a comprehensive investigation of the effect of physical parameters on the resonant frequency where left-handed characteristics occur. Model design and simulation were conducted in ANSYS High-Frequency Structure Simulator (HFSS) to extract the transmission coefficient and reflection coefficient while realizing negative permeability at a resonant frequency (f_o) of 1.2MHz. To further mitigate the resonant frequency of the MTM, a metaheuristic-based parameter optimization algorithm was implemented to achieve negative permeability and evanescent wave amplification at a resonant frequency of 750kHz, making it suitable for high-power WPT applications. A prototype MTM sample is fabricated for experimental measurement of power transfer efficiency and medium parameters, using the Keysight ENA5061 Vector Network Analyzer (VNA), effectively confirming the validity of the proposed design. The excellent efficiency enhancement and mutual coupling make the design an attractive solution for WPT applications. A close agreement between the experimental results and numerical simulation validates the accuracy of the optimization results.

INDEX TERMS Wireless power transfer, finite element analysis (FEA), metamaterial (MTM), power transfer efficiency, ANSYS, high frequency structure simulator, vector network analyzer, optimization.

I. INTRODUCTION

Wireless Power Transfer (WPT) has been widely studied and implemented in various applications, including mobile computing [1], wireless charging of biomedical body implants [2], and Electric Vehicles (EV) [3]. This technology was first discovered by Nikola Tesla in 1891 [4], and since then, significant research progress has been made. In 2007, researchers at MIT demonstrated the potential for efficient long-distance wireless power transmission using magnetic resonant coupling [5], and recently, Oak Ridge National Laboratory designed a 120-kilowatt WPT prototype for the wireless

The associate editor coordinating the review of this manuscript and approving it for publication was Diego Masotti.

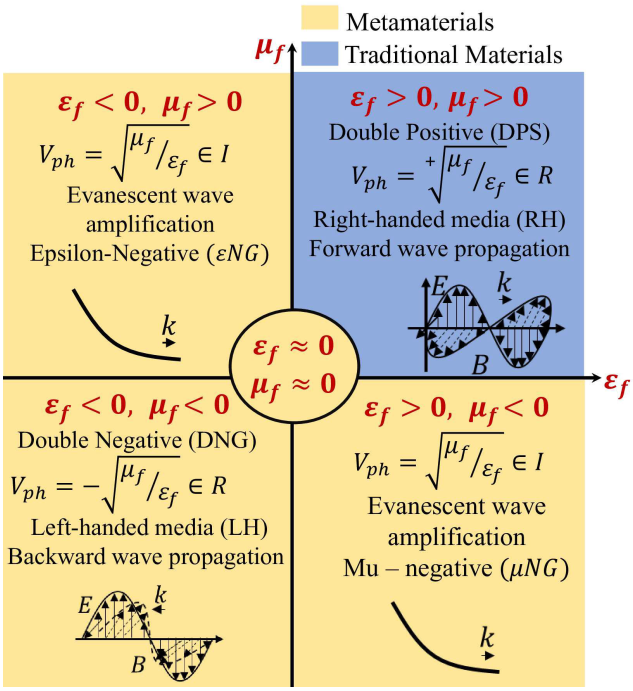

FIGURE 1. Schematic showing the categorization of Metamaterial (MTM) contingent on effective permeability(μ_f) and effective permittivity (ϵ_f) polarity. The electric field, magnetic field, wave number, and phase velocity, are denoted as E, B, k, V_{ph}, respectively.

charging of EV. However, there are still challenges to be addressed to fully realize the potential of WPT, including limited efficient magnetic resonant coupling distance and the inherent dependence of power transfer efficiency (PTE) on the coupling coefficient (k). Metamaterials (MTM) have emerged as promising candidates for enhancing WPT performance over a wide transfer distance. First described by Veselago in 1968 [6], MTM represents a generic term for materials with negative refractive index and perfect lensing (negative permittivity and permeability ($\epsilon_f < 0$; $\mu_f < 0$)) as exemplified in Eq. (1)

$$n = -\sqrt{\mu_f \epsilon_f} \tag{1}$$

The broad categorization of MTMs is shown in Fig. 1. While negative (DNG) MTM demonstrates negative effective permeability ($\mu_f < 0$) and negative effective permittivity ($\epsilon_f < 0$) for backward wave propagation, double positive (DPS) materials (forward wave media) are characterized by $\mu_f > 0$ and $\epsilon_f > 0$. However, in extremely sub-wavelength regions, there is a separation between the electric and magnetic fields, allowing the amplification of the evanescent wave and the attainment of a negative refractive index ($n < 0$).

To achieve practical low-frequency MTM structures with valid medium parameters, the MTM unit cell must satisfy the homogenization criterion, which specifies a small sample size ($l \ll \lambda$) compared to the wavelength at the operating frequency [7], [8], [9], [10], [11], [12], [13]. Numerous MTM designs and geometries have been reported in the literature to improve the performance of wireless power transfer (WPT). For example, in [14], split ring/spiral printed resonators and rectangular spiral-based MTM structures are discussed in detail, while [15] utilizes a multi-layer array of rectangular spiral for maximizing power transfer coupled with the enhancement of the power transmission efficiency (PTE). In [16], an effective MTM design for enhancing WPT performance is analyzed. Furthermore, [17] explores a planar hybrid MTM structure that integrates zero-permeability ($\mu_f = 0$) and negative permeability ($\mu_f < 0$) MTMs to reduce leakage EMF and increase transmit power. Moreover, [18], [19], [20], [21] comprehensively investigates various low-frequency MTMs that rely on the tuning of physical parameters. Although these MTM-based WPT designs exhibit superior performance in comparison to conventional coil structures, nonetheless, they typically resonate at significantly high radio and microwave frequencies, which is unfavorable for high-efficiency WPT applications [22], [23], [24]. In general, high resonant frequency results in high voltage and current stresses on passive components while also subjecting power semiconductor/MOSFET to high switching stress, leading to increased power dissipation, low efficiency, and degradation in WPT performance [10], [22], [23], [24], [25], [25], [26], [27].

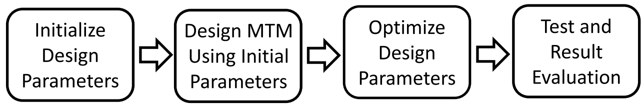

FIGURE 2. Schematic summary of design implementation process.

In this study, a low-frequency thin-PCB Metamaterial structure is studied alongside an optimization algorithm to analyze the impact of physical parameters on the resonant frequency in which evanescent wave amplification occurs. The proposed MTM structure stands out due to the unique way its individual layers are connected to achieve a constructive addition of magnetic flux. The main objective of this research is to investigate a left-handed MTM and decrease its evanescent resonant frequency to the kHz range, while simultaneously enhancing the PTE. A schematic representation of the model implementation steps is provided in Fig. 2.

The main contributions of this paper are summarized as follows:

i To design a miniaturized, thin PCB metamaterial (MTM) that operates at low frequencies for efficient wireless power transfer.
ii To develop an optimization algorithm to reduce the resonant frequency of the proposed MTM.
iii To experimentally validate the accuracy of the optimization algorithm using a prototype of the fabricated MTM sample

II. ANSYS HFSS ELECTROMAGNETIC SIMULATION AND METAMATERIAL CHARACTERIZATION

A. SYSTEM DESCRIPTION AND ELECTROMAGNETIC SIMULATION

The proposed MTM design is depicted in Fig. 3(a). Its layered rectangular spirals are orientated in opposite directions (The

TABLE 1. Parameter Specification Proposed MTM Unit cell.

Parameter	Unit	Value
Inter-turn spacing (Δr)	mm	1.6
Wire width (t)	mm	1.9
Litz wire guage	-	26 AWG, Unserved Single Build, 16 / 38 strand
Length (l)	mm	64
Dimension	mm^3	$64 \times 32 \times 3$

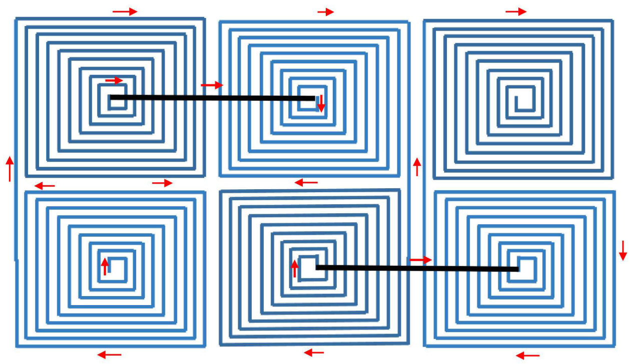

(a) Schematic of the Proposed MTM. The middle layer is a mirror image of both the first and third layer. The individual layers are connected in series to form a unit cell. Red arrows typify the direction of magnetic flux

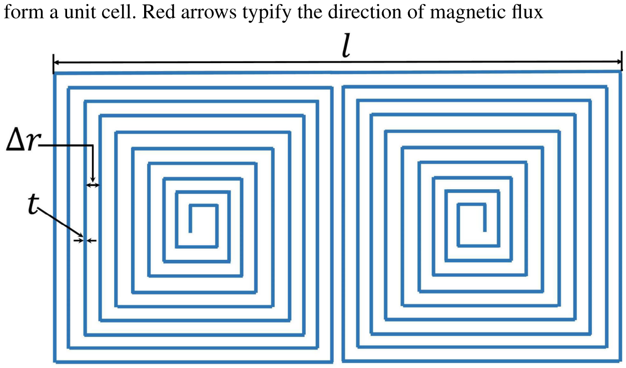

(b) Fundamental Component of the proposed metamaterial

FIGURE 3. Proposed metamaterial-based WPT Structure and its basic composing unit.

middle layer is a mirror image of the first and third layers) and also connected in series to achieve a constructive addition of the magnetic field. Apparently, the red arrow indicates the direction of travel of the magnetic flux. The series connection of the three layers constitutes an MTM unit cell. Similarly, Figure. 3(b) shows the fundamental layer of the proposed MTM in Fig. 3(a). Typically, each layer of the MTM is characterized by a wire thickness, t, an inter-turn spacing, Δr, and a length, l, which represents the maximum length of the unit cell. In addition, Table 1 denotes the parameter specification of the proposed unit MTM structure. A quantitative analysis of the impact of design parameters on the left-handed characteristics and resonant frequency of the proposed MTM structure is carried out using the finite element solver in ANSYS HFSS.

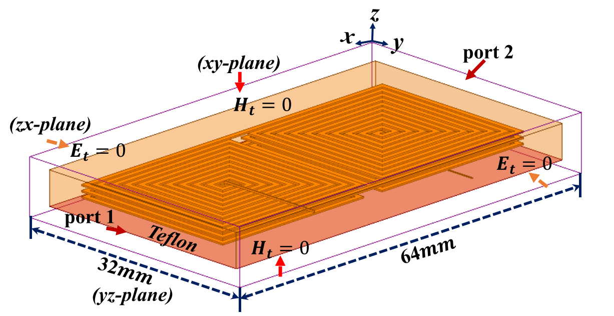

FIGURE 4. Configuration of unit metamaterial in a Full-wave ANSYS HFSS simulation. The setup includes the assignment of boundary conditions and excitation ports.

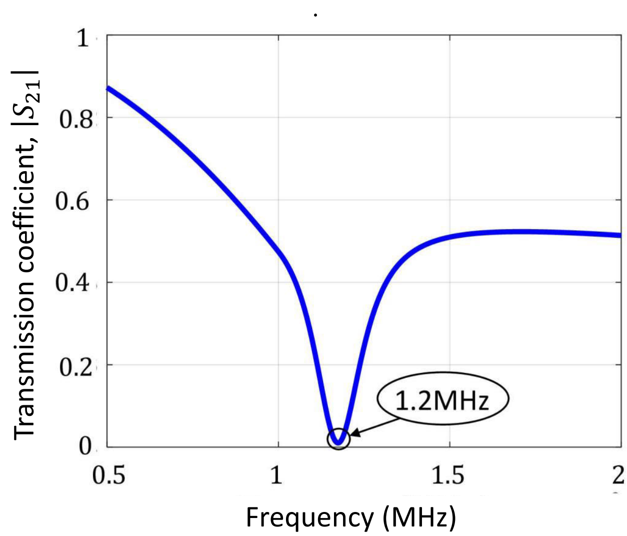

FIGURE 5. Extracted Transmission coefficient (S_{21}) of the proposed metamaterial, indicating evanescent wave amplification at $f_o = 1.2$ MHz.

As shown in Figure. 4, the simulated unit cell is enclosed in a Teflon substrate, having a high dielectric permittivity ($\epsilon_r = 4.4$) and low loss tangent ($tan\delta = 0.0004$).

In addition, perfect electric ($E_t = 0$) and perfect magnetic ($H_t = 0$) boundary conditions were applied to terminate the MTM along the y-axes and z-axes, respectively. Moreover, excitation is assigned to the boundary along the x-axis using externally applied waveguide ports. The excitation creates a magnetic field around the MTM unit cell. Using an extraction distance equal to the length, l, of the MTM coupled with the simulated transmission coefficient (S_{21}), and reflection coefficient (S_{11}) holistically referred to as scattering parameters, both the effective permeability (μ_f) and effective permittivity (ϵ_f) were retrieved based on Kramar-Kronig parameter retrieval algorithm [28]. The de-embedded simulated scattering parameter, S_{21} and S_{11} are shown in Fig. 5 and Fig. 6, respectively. Ostensibly, the proposed MTM exhibits a resonance frequency, $F_r = 1.2$ MHz, a significantly low frequency compared to the Gigahertz frequency of existing MTM structures. Additionally, the retrieved μ_f and ϵ_f plots depicted in Fig. 7 and Fig. 8, respectively demonstrate

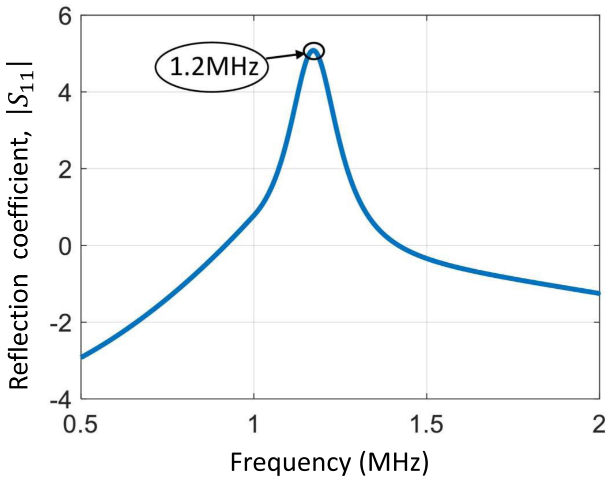

FIGURE 6. Extracted metamaterial reflection coefficient, showing low-frequency evanescent wave amplification. The metamaterial resonates at a frequency, $f_o = 1.2$ MHz.

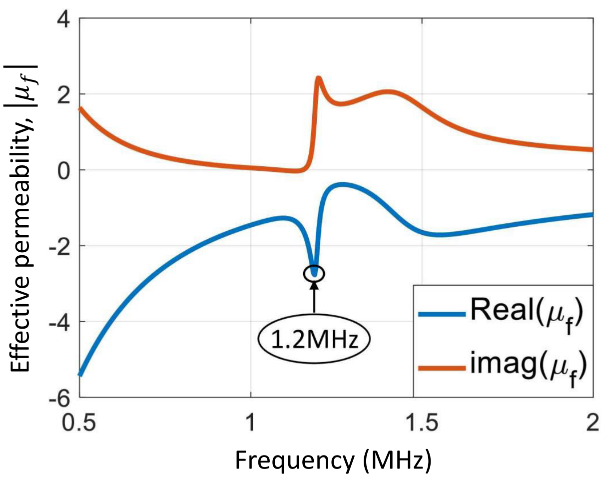

FIGURE 7. Retrieved permeability of proposed metamaterial, showing left-handed characteristics at a resonant frequency, $f_o = 1.2$ MHz.

1.2 MHz resonant frequency consistent with Fig. 5 and Fig. 6. Thus, the resonance frequency of μ_f, ϵ_f, S_{21}, and S_{22} are closely matched. In addition, the MTM demonstrates a negative real component of μ_f, corresponding to -2.8 at the resonant operating point, effectively confirming the validity of the MTM. Moreover, at the resonant frequency, the ratio of the electromagnetic wavelength and the length of the MTM unit cell (λ_o/l), which typifies a metric for appraising the compactness of MTM structures is evaluated as 3906, making it the most compact unit cell. A comparison of the proposed MTM and other existing MTM structures is shown in Table 2. Apparently, the proposed MTM demonstrates a very compact and miniaturized structure.

B. ELECTROMAGNETIC SIMULATION AND FINITE ELEMENT ANALYSIS

In order to investigate the performance enhancing capability of the proposed MTM, an MTM-slab based on a

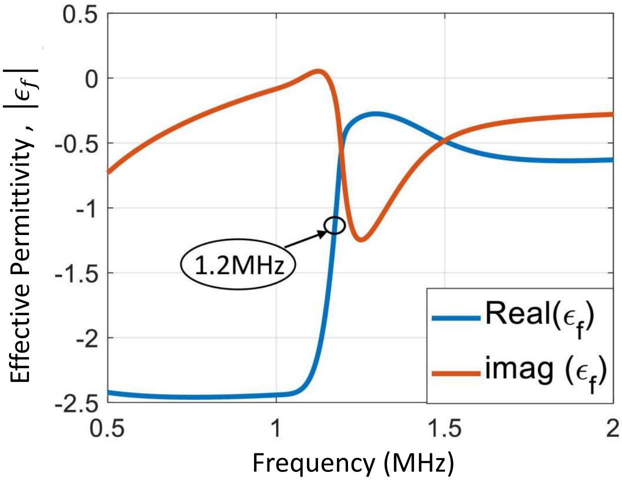

FIGURE 8. Retrieved permittivity of the proposed metamaterial, exhibiting left-handed characteristics at a resonant frequency, $f_o = 1.2$ MHz.

TABLE 2. Comparison of Wavelength to Length Ratio ($\frac{\lambda_o}{L}$) between existing Works and the Proposed Metamaterial.

Reference	[14]	[29]	[30]	Proposed MTM
Lateral size $\left(\frac{\lambda_o}{l}\right)$	170	300	442.8	3906
Resonant frequency	8.69 MHz	8.42 MHz	7.49 MHz	745.5 kHz

4×4 periodic array of unit MTM is integrated with a conventional two-coil WPT structure as displayed in Figure 9. Both the transmitter (Tx), and receiver (Rx) are made of three turns, 24AWG solid strand copper wire, having a coil radius of 100 mm; inductance, 10 nH; loaded chip capacitance; 100 pF, and an ohmic resistance of 0.0025 Ω. The aforementioned simulation parameters are in agreement with 5% maximum harmonic content for ripple minimization based on IEEE standard recommendation [22]. For performance comparison purposes, two full wave simulations were conducted in ANSYS electromagnetic simulator, first for the classical WPT system without MTM followed by the proposed MTM-incorporated WPT structure.

To preserve the working distance as well as prevent the intersection of the structures, a distance of 0.5 mm is maintained between transmitter (Tx) and MTM as well as receiver (Rx) and MTM while varying the working distance (MTM to MTM separation) from 50 mm to 250 mm. Moreover, it was determined based on ANSYS electromagnetic simulation that a 0.5 mm minimum distance is critical to preventing the intersection of the Tx and MTM as well as Tx and MTM. Besides, it is worth noting that attaching the MTM to the surface of either Tx or Rx effectively places the MTM on the flux traveling path, potentially enhancing leakage magnetic field and reduction in power transfer efficiency. Lastly, the power transfer efficiency of both the WPT system with and without metamaterial is analyzed for performance comparison.

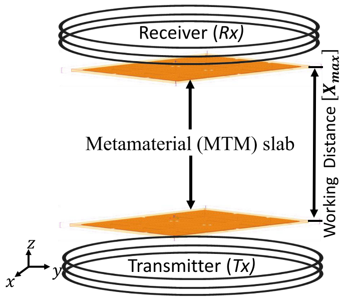

(a) With Metamaterial

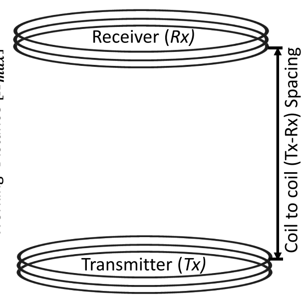

(b) Without Metamaterial

FIGURE 9. **ANSYS HFSS 3D simulation schematic of the proposed MTM-based WPT system. A separation of 0.5 mm is maintained between Tx - MTM and Rx - MTM to prevent a potential intersection. Each slab comprises a 4 × 4 array of unit MTM with a dimension of 256 × 96× 3 mm^3.**

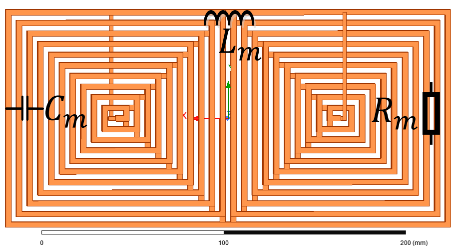

(a) Schematic of the proposed MTM unit cell based on ANSYS HFSS

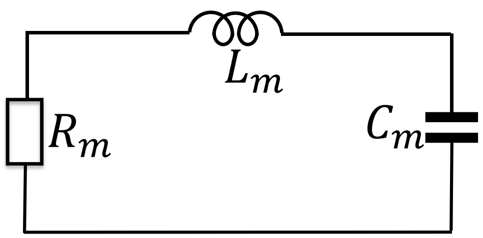

(b) Equivalent RLC lumped circuit representation of the proposed MTM

FIGURE 10. **Frontal Section of proposed MTM unit cell as designed in ANSYS HFSS and equivalent $R_m L_m C_m$ lump circuit.**

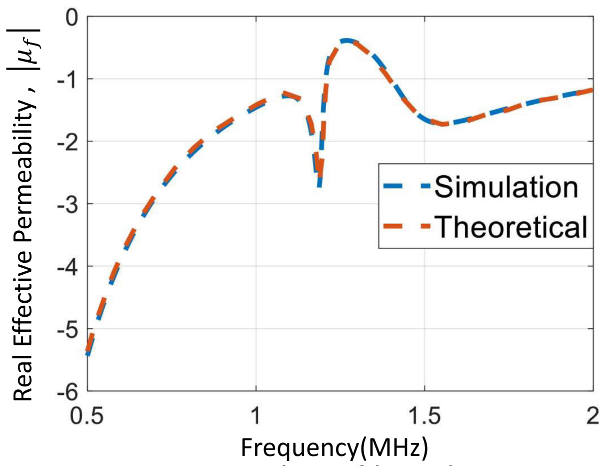

(a) Effective Permeability (μ_f)

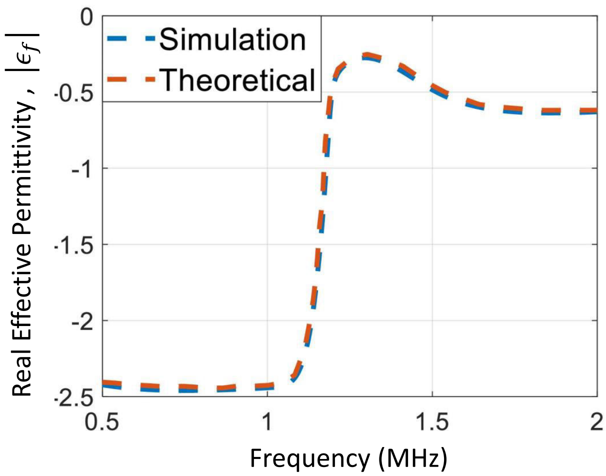

(b) Effective Permittivity (ϵ_f)

FIGURE 11. **Performance comparison of effective permeability (μ_f) and permittivity (ϵ_f) based on full-wave simulation and analytical models. A close correlation of both μ_f and ϵ_f validates the accuracy of the analytical model.**

III. PHYSICS-BASED MODELING AND METAHEURISTIC OPTIMIZATION OF PROPOSED METAMATERIAL FOR RESONANT FREQUENCY REDUCTION

This research combines physics-based modeling with metaheuristic-based optimization to analyze how the physical parameters of a proposed metamaterial (MTM) structure affect its resonant frequency. The main objective is to reduce the resonant frequency where evanescent wave amplification occurs. To achieve this goal, the study utilizes a Jaya-based optimization algorithm to optimize the lumped capacitance and stray inductance of the MTM, which have a comprehensive impact on the resonant frequency of the structure.

A. PHYSICS-BASED EXTRACTION OF MEDIUM PARAMETERS AND PERFORMANCE COMPARISON

The proposed unit cell in Figure 10(a) has been represented as an equivalent circuit model with a coupling coil composed of resonant parameters R_m, L_m, and C_m [9], [10], as shown in Figure 10(b). The lumped circuit inductance, capacitance, and resistance are denoted by L_m, C_m, and R_m, respectively. Equation (2) expresses the resistive parameter Rm of the unit cell as the sum of the lumped circuit resistance R_o, dielectric loss R_{dt} due to the copper coil, proximity loss R_{prox}, and skin effect loss R_{sk}. As exhibited in Eq. (2), the resistive parameter R_m, of the unit cell is expressed as the sum of the lumped circuit resistance (R_o), dielectric loss (R_{dt}) due to the copper coil, proximity loss (R_{prox}), and skin effect loss (R_{sk}).

$$R_m = R_{sk} + R_{prox} + R_{dt} + R_o \tag{2}$$

Moreover, R_{sk} is estimated as illustrated in Eq. 3

$$R_{sk} = R_{mc} \frac{t}{\delta\left(1 - e^{-\left(\frac{t}{\delta}\right)}\right)\left(1 + \frac{t}{\Delta r}\right)} \tag{3}$$

where $R_{mc} = \frac{l}{\sigma t \Delta r}$; σ is the conductivity of the wire; t - thickness of the wire; l - length of rectangular spiral, and δ is the skin depth as denoted in Eq. 4.

$$\delta = \sqrt{\frac{1}{\pi \mu f_r \sigma}} \tag{4}$$

where μ is the permeability of the MTM. The proximity loss, R_{prox}, which arises from the interaction between the fields of each wire turn, can be expressed mathematically as:

$$R_{prox} = 0.1228\, R_{dc} \left(\frac{\mu \Delta r \pi f_r}{R_{sh}}\right)^2 \tag{5}$$

Moreover, the resistance due to the dielectric material (R_{dt}) and the length of the spiral conductor can be expressed as demonstrated in Equation (7) and Equation (6), respectively

$$l = 4(\Delta r - tN)(N-1) - 4tN(N+1) \tag{6}$$

$$R_{dt} = \frac{tan\delta}{2\pi f_r C_s} \tag{7}$$

It's worth noting that tanδ is the loss tangent of the Teflon substrate and N is the number of spiral rectangular turns. Subsequently, the lumped circuit capacitance (C_m) of the metamaterial (MTM) unit cell denoted in Equation. (8) is represented by combining the compensation capacitor (C_{com}) and the stray capacitance (C_s) shown in Equation. (9).

$$C_s = \left[\frac{9}{10}\epsilon_{ar}\epsilon_o + \left(\frac{\epsilon_{tf}\epsilon_o}{10}\right)\left(\frac{t}{\Delta r}\right)l\right] \tag{8}$$

$$C = C_s + C_{com} \tag{9}$$

where ϵ_{ar} and ϵ_{tf} are the relative permittivity of air and Teflon substrate, respectively. It is worth stating that the resonant frequency of the MTM can be tuned by varying the value of C_{com}, accordingly. Further, the relationship between the lumped circuit inductance, L_m, of the unit MTM cell and the number of wire turn, N, is demonstrated in Eq. 10.

$$L_m = \frac{1.27\mu N^2 d_{av}}{2}\left[ln\left(\frac{2.07}{\Theta}\right) + 0.18k + 0.13\Theta^2\right] \tag{10}$$

where Θ is the fill ratio and the average length, d_{av}, and k are given by Eq. 11 and Eq. 12, respectively.

$$d_{av} = \frac{\Delta r + t}{2} \tag{11}$$

$$k = \frac{\Delta r + t}{\Delta r - t} \tag{12}$$

Essentially, the holistic combination of L_m and C_m in the form of $L_m C_m$ circuit resonance culminates in the resonant frequency, F_r, of the proposed MTM consistent with Eq. 13

$$F_r = \frac{1}{2\pi\sqrt{L_m C_m}} \tag{13}$$

The performance comparison of real effective permeability (μ_f) and permittivity (ϵ_f) of the proposed MTM based on full-wave HFSS simulation and derived analytical models are presented in Fig. 11(a) and Fig. 11(b), respectively. From the results, it can be inferred that the simulated and theoretical results for both μ_f and ϵ_f are in close agreement, effectively validating the accuracy of the theoretical model. Moreover, the resonance frequency of the simulated and analytical real component of μ_f and ϵ_f are closely matched at ≈1.2 MHz. Furthermore, both the simulation and theoretical results exhibit negative real components of μ_f and ϵ_f at their respective resonance frequency, essentially verifying the left-handed behavior of the proposed MTM structure.

B. JAYA-BASED OPTIMIZATION OF METAMATERIAL DESIGN PARAMETERS FOR RESONANT FREQUENCY REDUCTION

The Jaya-based optimization algorithm [31] proposed in this study harnesses a population-based optimization algorithm to find the global minimum or maximum of the function in Eq. (14) [32]. It works by maintaining a population of candidate solutions while also iteratively updating them to find the best solution. The update rule works by moving each candidate solution towards the best solution in the population, and the movement is proportional to the distance between the two solutions. This ensures that the solutions move towards the global optimum, even when the population has converged to a local optimum.

Given the MegaHertz resonant frequency behavior of the proposed MTM (specifically, 1.2 MHz) in ANSYS EM simulations, the overarching objective of this section is to develop an optimization algorithm capable of mitigating its resonant frequency to the Kilohertz range. Due to the complex relationship between the effective permeability (μ_f) and physical parameters of the proposed MTM, it is formulated as an optimization problem exhibited in Eq. 14. This equation expresses the dependence of μ_f and resonant frequency, F_r, on the physical parameters of the MTM, including inter-turn spacing (Δr), number of turns of copper wire (N), and copper wire thickness (t).

$$\mu_f(\Delta r, N, t) = 1 - \left[\frac{\left[\frac{l}{t}\right]^2}{1 + \frac{\rho}{\pi \Delta r F_r \mu_o (N-1)} - \frac{c_o^2}{l^2 \Delta r (N-1)}}\right] \tag{14}$$

where c_o is the speed of light, ρ is the resistivity of copper wire. The optimization objective is to reduce the resonant frequency where evanescent wave amplification (negative permeability, μ_f) occurs in the proposed MTM.

1) DESIGN PARAMETER OPTIMIZATION CONSTRAINT

To ensure the optimized MTM can be implemented in a practical manner, three objective variables are considered for the analysis: Δr, N, and t, as described in Equation (15)

$$F_r = f(\Delta r, N, t) \tag{15}$$

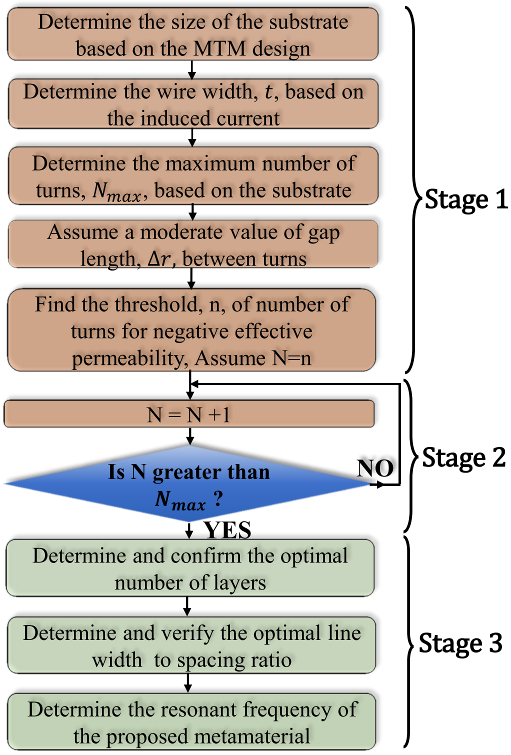

FIGURE 12. **Flowchart Architecture of Proposed Optimization Algorithm for reducing the resonant frequency of the proposed metamaterial.**

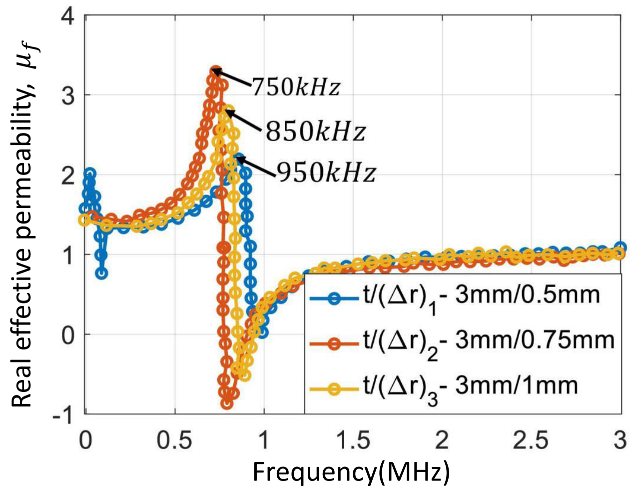

FIGURE 13. **Metamaterial effective permeability, showing the impact of optimizing structural parameters on the resonant frequency and evanescent wave amplification.**

where the resonant frequency, F_r represents the objective function.

In perspective, the optimization problem to be solved is a minimization of the given relation in Eq. (16). The constraints for each variable are also illustrated

$$\begin{aligned} &min \quad f(\Delta r, N, t) \\ &s.t. \quad \Delta r_{min} < \Delta r \leq \Delta r_{max} \\ &\qquad N_{min} < N \leq N_{max} \\ &\qquad t_{min} < t \leq t_{max} \end{aligned} \tag{16}$$

It is noteworthy that the physical parameters of a metamaterial, specifically N and Δr, have a significant impact on the inductance (L_m) and capacitance (C_m), respectively, which consequently affect the resonant frequency of the MTM. Therefore, optimizing these parameters can potentially lower the resonant frequency, as shown in Eq. (15). The design constraints provided below take these factors into consideration:

1) The inter-turn spacing or clearance between adjacent turns, denoted by Δr, is crucial for controlling the parasitic capacitance and leakage electromagnetic field of the resonator. The optimized value of Δr is chosen such that it is less than or equal to the original clearance, denoted by Δr_{max}, between adjacent turns before optimization.
2) The number of wire turns, denoted by N, is chosen consistently with the area of the proposed MTM, denoted by A_1, and the size of the substrate, denoted by A_2. The optimal number of turns is determined such that N is greater than or equal to the actual number of wire turns, denoted by N_{max}, and the areas of the MTM and substrate are less than or equal to their respective maximum values, denoted by A_{1max} and A_{2max}, prior to optimization.
3) The wire thickness, denoted by t, is estimated based on the target transmit power, which consequently determines the maximum excitation current based on the wire ampacity. In perspective, the minimum thickness of wire is selected to withstand the ampacity such that t is less than or equal to the initial wire thickness prior to optimization (t_{max}).

Figure 13 illustrates an implementation flowchart of the optimization procedure which is divided into three stages, namely Stage1, stage2 and stage3.

In stage 1, the initial values of key structure parameters/objective variables, such as wire thickness (t), number of turns (N), and inter-turn spacing (Δr), are chosen based on practical applications. The optimization algorithm iteratively adjusts the wire thickness until an optimal value that can handle the ampacity is obtained. The number of turns, N, is determined using the area of the MTM and substrate size, while a moderate value of r is used to minimize parasitic effects and stray magnetic fields.

In stage 2, a moderate number of turns is determined iteratively consistent with the MTM's area and substrate size while checking the corresponding resonant frequency. Finally, stage 3 investigates the optimized design parameters while tuning other parameters to achieve optimal results. Figure 14 demonstrates the effect of optimized design parameters of the MTM on the effective permeability and resonant frequency of the structure. Figure. 13.

In perspective, for a fixed wire width, t = 3 mm and inter-turn spacing, Δr iterated from 0.5 mm to 1 mm at an offset

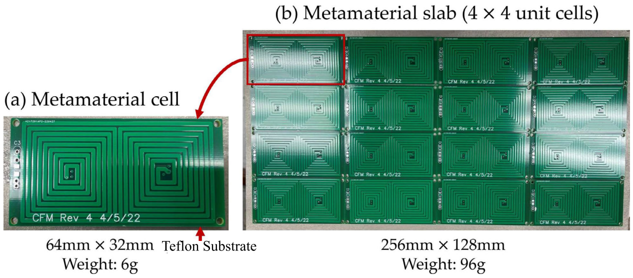

FIGURE 14. **Fabricated prototype of the proposed metamaterial (MTM) structure, indicating the Unit MTM and an MTM-slab based on a periodic 4 × 4 array of unit cell.**

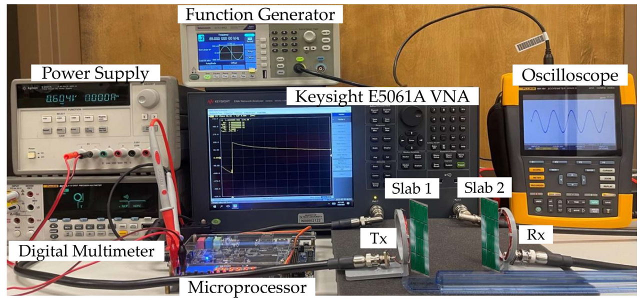

FIGURE 15. **Hardware set-up of the proposed WPT system incorporating MTM slab showing Keysight ENA 5061A Vector Network Analyzer. Tx and Rx positions are kept constant while varying the position of Slab 1 relative to slab2.**

of 0.25 mm, it is observed that the MTM effectively exhibits negative real permeability at resonant frequencies 750 kHz and 850 kHz corresponding to $\Delta r_1 = 0.5$ mm and $\Delta r_3 = 1$ mm, respectively, whereas $\Delta r_2 = 0.75$ mm demonstrates positive permeability. The aforementioned apparently shows that an optimal selection of $\frac{t}{\Delta r}$, does effectively minimizes resonant frequency while also influencing its evanescent wave amplification property. While the optimization process yielded three resonant frequency points as shown in Figure 13, only the design parameters corresponding to the lowest optimal resonant frequency (750 kHz) was harnessed for the experimental prototype. Moreover, the selection of 750 kHz frequency is based on practical integration with wireless charging systems that operate at 85 kHz, consistent with Airfuel Alliance Standard [33], [34]. The optimal design parameters for the 750 kHz resonant frequency were used to fabricate the MTM structure, and experimental testing was conducted to verify the accuracy of the optimization process, as described in Section IV.

IV. EXPERIMENTAL MEASUREMENT AND PERFORMANCE VALIDATION

In order to experimentally validate the proposed MTM, a prototype sample was fabricated as shown in Figure 14, and performance measurements were conducted using the prototype testbench shown in Figure 15. The MTM-slab, which consisted of a 4 × 4 periodic MTM array, was constructed using PCB technology and single-strand copper wires of 26 AWG, and positioned on a 1mm thick Teflon substrate to securely hold the copper wires. Moreover, compensation capacitors were soldered beneath the PCB board based on the specifications in Table 3.

Furthermore, the Tx-coil and Rx-coil were connected to port 1 and port 2 of the KeySight EN5061A Vector Network Analyzer (VNA) using 50Ω micro SMA connections. External holes were created in the substrate slab to provide a support framework for the experimental set-up. Measurements are taken using both port 1 and port 2 of the VNA to measure the transmission coefficient, S_{21}, reflection coefficient, S_{11}, and Z-parameters. The MTM slabs were then combined with the two coil structures shown in Figure 15 while taking measurements for sweep values of the working distance (slab1 to slab 2 distance) ranging from 50 mm to 250 mm. To prevent the slab1 and slab2 from potentially intersecting the Rx-coil and Tx-coil, respectively, the distance between both the Tx-coil and slab1, as well as Rx-coil and slab2, was kept at 0.5mm while retaining the working distance/loading position as depicted in Figure 15. The Tx-coil was stimulated using a start frequency of 100 kHz (0.1 MHz), a stop frequency of 10 MHz, and 671 data points. The collected data including the scattering parameters (S_{21} and S_{11}), Z-parameters, and working distances were analyzed to determine the power transfer efficiency (PTE) of the proposed system. In order to compare performance, an identical testing technique was performed on the WPT system without the MTM-slab.

TABLE 3. **Experimental design parameters.**

Parameter	Metamaterial	Transmitter	Receiver
Turns	10	3	3
Inner diameter	N/A	20 mm	20 mm
Outer diameter	N/A	30 mm	30 mm
Trace Width	2 mm	2 mm	2 mm
Copper wire guage	-	26 AWG	26 AWG
Capacitance (C_{com})	600 pF	N/A	N/A
Size	$64 \times 32 \times 3$ mm^3	N/A	N/A
Substrate	Teflon	PLA	PLA

V. PROTOTYPE MEASUREMENTS AND DISCUSSION OF RESULT

The main objective of this section is to experimentally validate the resonant operating frequency of the proposed MTM. Based on the prototype set-up in Fig 14 and Fig. 15, the experimentally retrieved transmission coefficient (S_{21}) and reflection coefficient (S_{11}) of the proposed MTM exhibit resonant behavior at a frequency of 743.5 kHz. It is apparent that this frequency is closely related to the resonant frequency obtained from the optimization result, effectively validating the accuracy of the optimization algorithm. In addition, it is noteworthy that the resonant frequency of the proposed MTM is significantly lower in comparison to the resonant frequencies of existing MTM designs, thus making it an attractive candidate for high-efficiency wireless charging applications.

Furthermore, when the loading position of slab 1 relative to slab 2 is varied from 50 mm to 250 mm and the

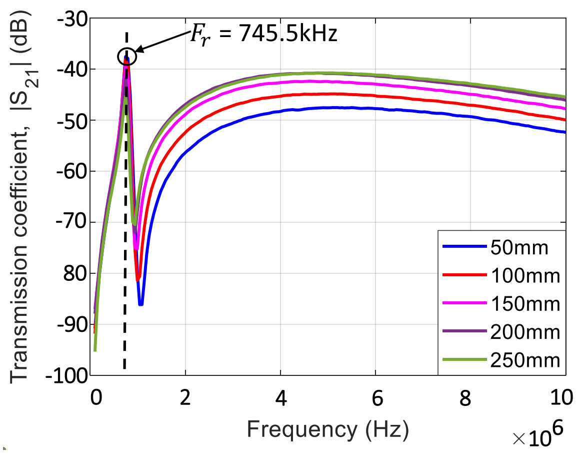

FIGURE 16. **Experimental waveform of the proposed MTM's Transmission coefficient (S_{21}). For all working distance ranging from 50 mm to 250 mm, the MTM resonates at a frequency, $F_r = 745.5$ kHz.**

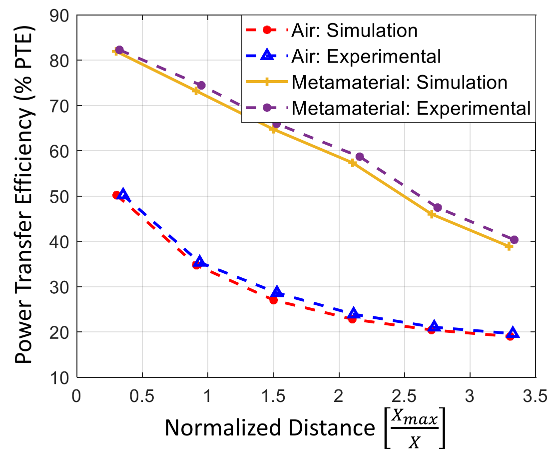

FIGURE 18. **Performance comparison of experimential and simulated WPT efficiency with and without MTM.**

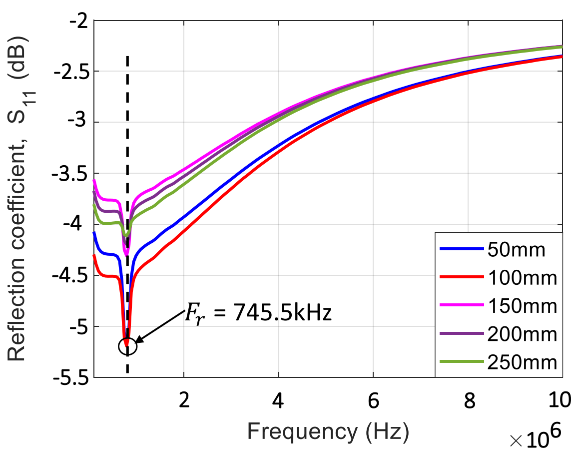

FIGURE 17. **Experimental waveform of the proposed MTM's reflection coefficient (S_{11}). The MTM shows a resonant behaviour at $F_r = 745.5$ kHz for all working distance ranging from 50 mm to 250 mm.**

separation/offset between both Tx and slab1, as well as Rx and slab2, is fixed at 0.5 mm, the resonant frequency of the MTM remains fairly constant at 743.5 kHz, as indicated by the plots of S_{21} and S_{11} corresponding to Figure 16 and Figure 17, respectively. The magnitude of S_{21} and S_{11} is significantly influenced by the loading position, while the resonant operating frequency remains constant.

A. MEASUREMENT OF TRANSFER EFFICIENCY (η) OF PROPOSED METAMATERIAL BASED WPT STRUCTURE

Consistent with [35] and [10], the power transfer efficiency (η) was investigated using the experimentally extracted Z-parameters (using the prototype test-bench in Figure 15) and the expression in Eq. (17),

$$\eta = \frac{|Z_{21,\text{ef}}|^2}{\Re\{Z_{11,\text{ef}}\}R_L} \times 100 \quad [\%]. \tag{17}$$

where $Z_{21,ef}$ is the extracted transmission Z-parameter from port 1 to port 2, whereas $Z_{11,ef}$ is the extracted reflection Z-parameter from port 1 to port 1. Further, experimental measurements were performed using the same working distance (MTM to MTM) distance harnessed for the ANSYS electromagnetic simulation. The simulated and experimental waveform of PTE as a function of normalized distance ($\frac{X_{max}}{X}$) for the system with and without MTM is exhibited in Fig. 18. The normalized distance is evaluated as the ratio of the maximum working distance, X_{max} (slab1 to slab2 distance), and parametric working distance (X) harnessed in the electromagnetic simulation. Apparently, the observed close matching of the simulation and experimentally measured transfer efficiency confirms the accuracy of the measurement results. The slight discrepancy could be traced to the inherent approximation in the computation of the lumped element impedances. Moreover, when the WPT system is integrated with two MTM slabs (each located close to the Tx and Rx), a significant increase in PTE for all normalized distances is observed compared to the WPT system without MTM.

VI. CONCLUSION

In this study, a metamaterial structure has been analyzed for low resonant behavior and evanescent wave amplification of a near magnetic field. Full-wave electromagnetic simulation has been performed in ANSYS HFSS electromagnetic solver culminating in design characterization based on extracted scattering parameters coupled with effective permeability and permittivity of the medium. Moreover, a meta-heuristic-based optimization of MTM physical parameters has been implemented to lower the resonant frequency of the MTM to 750kHz. The optimization analyzes the impact of design parameters on the resonant frequency where evanescent wave amplification occurs. Performance validation and verification of the accuracy of the optimization results with experimental measurements have been performed using a fabricated MTM sample. Apparently, the resonant frequency resulting from measurement per fabricated prototype closely matches the optimization result, essentially validating the accuracy of the optimization algorithm Thus, as a future extension of this work, advanced optimization algorithms are currently being developed to explore lower resonant frequency regions, preferably 85 kHz.

REFERENCES

[1] F. Zhang, X. Liu, S. A. Hackworth, R. J. Sclabassi, and M. Sun, ''In vitro and in vivo studies on wireless powering of medical sensors and implantable devices,'' in *Proc. IEEE/NIH Life Sci. Syst. Appl. Workshop*, Apr. 2009, pp. 84–87.

[2] R. Narayanamoorthi, ''Modeling of capacitive resonant wireless power and data transfer to deep biomedical implants,'' *IEEE Trans. Compon., Packag., Manuf. Technol.*, vol. 9, no. 7, pp. 1253–1263, Jul. 2019.

[3] J. Park, S. H. Kim, and O. Jeong, ''Use case and service framework for WPT (wireless power transfer),'' in *Proc. 16th Int. Conf. Adv. Commun. Technol.*, Pyeongchang, South Korea, 2014, pp. 1027–1030, doi: 10.1109/ICACT.2014.6779114.

[4] N. Tesla, ''Apparatus for transmitting electrical energy,'' U.S. Patent 1 119 732, Dec. 1, 1914.

[5] A. Kurs, A. Karalis, R. Moffatt, J. D. Joannopoulos, P. Fisher, and M. Soljačić, ''Wireless power transfer via strongly coupled magnetic resonances,'' *Science*, vol. 317, no. 5834, pp. 83–86, Jul. 2007.

[6] V. G. Veselago, ''Electrodynamics of substances with simultaneously negative permeability and permmitivity,'' *Uspekhi Fizicheskikh Nauk*, vol. 92, p. 517, Jan. 1967.

[7] W. Adepoju, I. Bhattacharya, M. Sanyaolu, and E. N. Esfahani, ''Equivalent circuit modeling and experimental analysis of low frequency metamaterial for efficient wireless power transfer,'' *IEEE Access*, vol. 10, pp. 87962–87973, 2022.

[8] W. Adepoju, I. Bhattacharya, M. Sanyaolu, M. E. Bima, T. Banik, E. N. Esfahani, and O. Abiodun, ''Critical review of recent advancement in metamaterial design for wireless power transfer,'' *IEEE Access*, vol. 10, pp. 42699–42726, 2022.

[9] W. Adepoju, I. Bhattacharya, I. Fidan, N. E. Ebrahim, O. Abiodun, R. Buchanan, T. Banik, and M. E. Bima, ''Equivalent circuit modeling and analysis of metamaterial based wireless power transfer,'' 2022, *arXiv:2210.03740*.

[10] W. O. Adepoju, ''Modeling, artificial intelligence-based optimization and experimental implementation of novel low-frequency metamaterial for efficient wireless power transfer,'' Tennessee Technol. Univ., 2022.

[11] W. O. Adepoju, I. Bhattacharya, M. E. Bima, and T. Banik, ''Novel metamaterial and AI-based multi-objective optimization of coil parameters for efficient wireless power transfer,'' in *Proc. IEEE Vehicle Power Propuls. Conf. (VPPC)*, Oct. 2021, pp. 1–6.

[12] M. E. Bima, I. Bhattacharya, W. O. Adepoju, and T. Banik, ''Effect of coil parameters on layered DD coil for efficient wireless power transfer,'' *IEEE Lett. Electromagn. Compat. Pract. Appl.*, vol. 3, no. 2, pp. 56–60, Jun. 2021.

[13] M. E. Bima, I. Bhattacharya, and C. W. V. Neste, ''Experimental evaluation of layered DD coil structure in a wireless power transfer system,'' *IEEE Trans. Electromagn. Compat.*, vol. 62, no. 4, pp. 1477–1484, Aug. 2020.

[14] B. Wang, K. H. Teo, T. Nishino, W. Yerazunis, J. Barnwell, and J. Zhang, ''Experiments on wireless power transfer with metamaterials,'' *Appl. Phys. Lett.*, vol. 98, no. 25, Jun. 2011, Art. no. 254101.

[15] W.-C. Chen, C. M. Bingham, K. M. Mak, N. W. Caira, and W. J. Padilla, ''Extremely subwavelength planar magnetic metamaterials,'' *Phys. Rev. B, Condens. Matter*, vol. 85, no. 20, May 2012, Art. no. 201104.

[16] E. S. G. Rodríguez, A. K. RamRakhyani, D. Schurig, and G. Lazzi, ''Compact low-frequency metamaterial design for wireless power transfer efficiency enhancement,'' *IEEE Trans. Microw. Theory Techn.*, vol. 64, no. 5, pp. 1644–1654, May 2016.

[17] K. B. Alici, F. Bilotti, L. Vegni, and E. Ozbay, ''Miniaturized negative permeability materials,'' *Appl. Phys. Lett.*, vol. 91, no. 7, Aug. 2007, Art. no. 071121.

[18] H. Wang, W. Wang, X. Chen, Q. Li, and Z. Zhang, ''Analysis and design of kHz-metamaterial for wireless power transfer,'' *IEEE Trans. Magn.*, vol. 56, no. 8, pp. 1–5, Aug. 2020.

[19] W. Adepoju, I. Bhattacharya, C. V. Neste, O. M. Sanyaolu, A. Olatunji, and T. Banik, ''Model based analysis of low frequency metamaterial for efficient wireless power transfer,'' in *Proc. IEEE Vehicle Power Propuls. Conf. (VPPC)*, Nov. 2022, pp. 1–7.

[20] A. Olatunji, I. Bhattacharya, W. Adepoju, E. N. Esfahani, and T. Banik, ''Application of artificial intelligence in optimization of solid state transformer core for modern electric vehicles using multi-objective genetic algorithm,'' in *Proc. IEEE Vehicle Power Propuls. Conf. (VPPC)*, Nov. 2022, pp. 1–7.

[21] E. N. Esfahani, I. Bhattacharya, W. Adepoju, and A. Olatunji, ''Modeling and tuning of parameters of a bidirectional wireless power transfer for interfacing EVs with the DC smart grids,'' in *Proc. IEEE Vehicle Power Propuls. Conf. (VPPC)*, Nov. 2022, pp. 1–6.

[22] A. W. Oluwafemi, E. Ozsoy, S. Padmanaban, M. S. Bhaskar, V. K. Ramachandaramurthy, and V. Fedák, ''A modified high output-gain cuk converter circuit configuration for renewable applications—A comprehensive investigation,'' in *Proc. IEEE Conf. Energy Convers. (CENCON)*, Oct. 2017, pp. 117–122.

[23] E. Ozsoy, S. Padmanaban, A. W. Oluwafemi, V. K. Ramachandaramurthy, and T. Sutikno, ''Modified (2/1-k) output gain Ćuk DC-to-DC converter circuit for renewable power applications,'' in *Proc. IEEE 12th Int. Conf. Compat., Power Electron. Power Eng. (CPE-POWERENG)*, Apr. 2018, pp. 1–6.

[24] A. Olatunji, I. Bhattacharya, and W. Adepoju, ''*WINNER* AI based optimization of solid state transformer core for modern electric vehicles using multi-objective genetic algorithm,'' *Proc. Student Res. Creative Inquiry Day*, vol. 6, p.1, May 2022.

[25] Z. Zhang, A. W. Oluwafemi, M. Hosseinzadehtaher, and M. B. Shadmand, ''Current observer based predictive decoupled power control grid-interactive inverter,'' in *Proc. IEEE Texas Power Energy Conf. (TPEC)*, Feb. 2020, pp. 1–6.

[26] W. Adepoju, I. Bhattacharya, M. E. Bima, and T. Banik, ''Modeling and performance comparison of GaN HEMT and SiC MOSFET for onboard charging application,'' in *Proc. IEEE 93rd Veh. Technol. Conf. (VTC-Spring)*, Apr. 2021, pp. 1–7.

[27] W. Adepoju, I. Bhattacharya, O. M. Sanyaolu, N. E. Ebrahim, and O. Abiodun, ''Modeling and theoretical investigation of grid-interactive ultracapacitor fuel-cell for renewable application,'' in *Proc. IEEE IAS Global Conf. Renew. Energy Hydrogen Technol. (GlobConHT)*, Mar. 2023, pp. 1–7.

[28] Z. Szabo, G. H. Park, R. Hedge, and E. P. Li, ''A unique extraction of metamaterial parameters based on Kramers–Kronig relationship,'' *IEEE Trans. Microw. Theory Techn.*, vol. 58, no. 10, pp. 2646–2653, Oct. 2010.

[29] A. L. A. K. Ranaweera, T. P. Duong, and J.-W. Lee, ''Experimental investigation of compact metamaterial for high efficiency mid-range wireless power transfer applications,'' *J. Appl. Phys.*, vol. 116, no. 4, Jul. 2014, Art. no. 043914.

[30] V. T. Nguyen, S. H. Kang, and C. W. Jung, ''Wireless power transfer for mobile devices with consideration of ground effect,'' in *Proc. IEEE Wireless Power Transf. Conf. (WPTC)*, May 2015, pp. 1–4.

[31] E. H. Houssein, A. G. Gad, and Y. M. Wazery, ''Jaya algorithm and applications: A comprehensive review,'' *Metaheuristics and Optimization in Computer and Electrical Engineering*. 2021, pp. 3–24.

[32] Z. Zhang and B. Zhang, ''Angular-misalignment insensitive omnidirectional wireless power transfer,'' *IEEE Trans. Ind. Electron.*, vol. 67, no. 4, pp. 2755–2764, Apr. 2020.

[33] W. Adepoju, I. Bhattacharya, and M. Bima, ''*WINNER* novel ferrite-core metamaterial and AI-based coil parameter optimization for efficient wireless power transfer,'' *Proc. Student Res. Creative Inquiry Day*, vol. 5, p. 1, Apr. 2021.

[34] E. N. Esfahani, I. Bhattacharya, and W. Adepoju, ''Simultaneous design of circular pad and double side compensation network for dynamic wireless power transfer,'' in *Proc. IEEE Int. Symp. Electromagn. Compat. Signal/Power Integrity (EMCSI)*, Aug. 2022, pp. 113–118.

[35] A. K. RamRakhyani and G. Lazzi, ''On the design of efficient multi-coil telemetry system for biomedical implants,'' *IEEE Trans. Biomed. Circuits Syst.*, vol. 7, no. 1, pp. 11–23, Feb. 2013.

WEBSTER ADEPOJU (Member, IEEE) received the B.Sc. degree in electrical and computer engineering from Obafemi Awolowo University, Nigeria, the M.E. degree (Hons.) in electrical and computer engineering from the University of Johannesburg, South Africa, and the Ph.D. degree in electrical and computer engineering from Tennessee Tech University, USA. From 2018 to 2019, he was a Research Assistant with the Centre for Telecommunications, University of Johannesburg, where he has investigated the effect of common mode and differential mode noise on cables used for power line communication. Prior to this, he involved in the modeling and control of high-gain dc–dc converters, observer-based sensor-less systems, and advanced model predictive control of single phase inverter. He is currently a Server CPU Validation Engineer with Intel Corporation. His current research interests include post-silicon validation and debugging, low frequency metamaterial-based wireless power transfer, power electronics, wide-band-gap devices, and semiconductor characterization. He was a recipient of the 2021 Best Poster Presentation Award from the University's Research and Creative Inquiry Day.

INDRANIL BHATTACHARYA (Senior Member, IEEE) received the B.E. degree (first class with distinction) in electronics and communication engineering from India and the M.S. and Ph.D. degrees in electrical engineering from Florida State University. He is currently a Professor and the Associate Chair with the Department of Electrical and Computer Engineering, Tennessee Technological University. He is the inventor of three U.S. patents. He has been the Principal Investigator of U.S. $3.6 million funding from agencies, like the National Science Foundation and the U.S. Department of Energy. He has published 58 peer-reviewed technical papers in reputed journals and conferences. He has supervised eight Ph.D., 14 master's, and 55 bachelor's students. His research interests include lithium and sodium-based battery technologies, high-efficiency III–V solar cells, wireless power transfer, and electromagnetics.

MARY SANYAOLU received the bachelor's degree from the University of Lagos and the master's degree from the University of Johannesburg, South Africa. From 2014 to 2015, she was an Intern with Oando Oil Corporation. From 2017 to 2021, she was with the University of Johannesburg. She is currently a Geo-Technical Engineer with GasFleet Engineering. Her current research interests include nano-materials, material characterization, modeling, and analysis. She was a recipient of the prestigious Global Excellence Scholarship and the National Research Fellowship.

MUHAMMAD BIMA ENAGI (Student Member, IEEE) received the B.Eng. degree in electrical and computer engineering from the Federal University of Technology, Minna, the M.Sc. degree in communication engineering from The University of Manchester, and the Ph.D. degree in engineering from Tennessee Technological University, with a focus on wireless power transfer. He was a Research Assistant with the SOLBAT-TTU Energy Research Laboratory. He also interned with the Research and Development Quality Assurance Unit, ANSYS Inc. He taught with the Department of Mechatronics Engineering, Federal University of Technology, Minna, where he mentored and taught students. He is currently a Software Engineer with Nordstrom Inc. He was a recipient of the College of Engineering Eminence Award for the Doctor of Philosophy Best Paper, in 2020, and the Best Poster Presentation Award from the 2020 and 2021 Research and Creative Inquiry Days at the University.

EBRAHIM NASR ESFAHANI received the B.S. degree in electrical engineering from the University of Kashan, Iran, in 2007, and the M.S. degree in electrical engineering from IAUN, Iran, in 2010. He is currently pursuing the Ph.D. degree in electrical and computer engineering with Tennessee Technological University, Cookeville, TN, USA. He was in the industry as an Electrical Maintenance Engineer with Steel Company for more than eight years. His research interests include the design and analysis of electric machines, the modeling of electromagnetic devices, and wireless power transfer.

TRAPA BANIK (Graduate Student Member, IEEE) received the B.S. degree from the Chittagong University of Engineering and Technology, Bangladesh. She is currently pursuing the Ph.D. degree in electrical and computer engineering with Tennessee Technological University, under the supervision of Dr. Indranil Bhattacharya. Her research interest includes sodium-ion battery, wireless power transfer, electric vehicle systems, renewable energy, and smart grid systems.

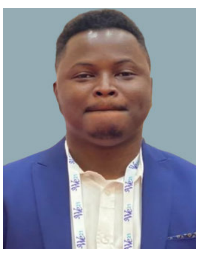

OLATUNJI ABIODUN (Graduate Student Member, IEEE) received the B.Sc. degree (Hons.) in electrical and electronics engineering from Obafemi Awolowo University, Nigeria. He is currently pursuing the master's degree with the Department of Electrical and Computer Engineering, Tennessee Technological University. He has six years industrial experience in electrical and electronics engineering related fields. His research interests include wireless power transfer, high-frequency transformers, and electric vehicles.